Magnetic Helical Robot for Targeted Drug-Delivery in Tubular Environments

Jaekwang Nam, Wonseo Lee, *Student Member, IEEE*, Jongyul Kim, and Gunhee Jang, *Member, IEEE*

***Abstract*—We propose a novel magnetic helical robot (HR) that can helically navigate, release a drug to a target area, and generate a mechanical drilling motion to unclog tubular structures of the human body. The proposed HR is composed of two rotating cylindrical magnets (RMs), four fixed cylindrical magnets (FMs), and a helical body. The RMs can be rotated in different directions under two orthogonal external rotating magnetic fields (ERMF). Utilizing these ERMFs, we can generate various motions. The ERMF along the axis of the RMs can generate the drug-release motion, while the ERMF orthogonal to the axis of the RMs can generate navigating and drilling motions. On the other hand, the magnetic torque and the attractive magnetic force between RMs and FMs tightly seal the nozzles in the drug chamber. We analyze these magnetic torque and force of the magnets for the navigating, drug-release, and drilling motion. Especially, the drug-release motion utilizes an eccentric rotational motion of the RMs due to the attractive and repulsive magnetic force between RMs and FMs. This motion squeezes and discharges the drug through a nozzle. We designed the mechanical structure of the proposed HR considering the magnetic properties to achieve the proposed functions. Finally, we prototyped the HR and conducted several experiments to verify the navigating, drug-delivery and drilling capabilities of the HR. We also confirmed that drug-enhanced drilling could unclog the clogged area more effectively than the simple drilling motion.**

***Index Terms*—Drug delivery systems, magnetic devices, magnetic fields, medical robotics, seals.**

I. Introduction

WIRED catheters are popular in modern surgical procedures for the treatment of clogged tubular structures in the human body, such as blood vessels and the gastrointestinal tract [1]–[4]. These surgeries are relatively simple and minimally invasive because medical doctors insert a catheter through a small hole and do several procedures without performing a laparotomy. However, medical doctors are continuously exposed to high doses of radiation when they perform angiography using an X-ray device to obtain images of the location of the catheter or target area [5]. Twisted and narrow tubular environments present another problem because it is difficult to smoothly steer the wired catheter in these complex environments.

Wireless magnetic robots and their associated magnetic navigation systems (MNSs) have been investigated as an alternative to the conventional procedures. Several researchers have studied MNSs [6], [7]. Choi *et al.* developed an MNS with two pairs of stationary Helmholtz coils, and two pairs of stationary Maxwell coils to control a magnetic helical robot (HR) [6]. Jeon *et al.* improved the MNS using uniform and gradient saddle coils [7]. The developed MNSs are structurally compact and can fit in the human body. Several researchers have investigated the control method utilizing the MNS. Ma *et al.* developed the robust feedback control method of the microparticle to accurately guide the microparticle [8]. Nam *et al.* proposed the control method utilizing a resonant effect of an RLC circuit to maximize the output current and the magnetic field without phase delay at variable resonant frequency [9]. Various magnetic robots, which are manipulated by the MNSs, also have been investigated, such as capsules, crawling robots, inchworms, earthworms, and HRs [10]–[15]. The HRs are some of the most promising magnetic robots because they have a simple structure and effective motion mechanism. In addition, the HR can drill the clogged area using a helical blade. Several researchers have focused on the drilling ability of the HR [12], [15]. Ishiyama *et al.* developed a simple HR and investigated the drilling ability of the HR for several design variables [12]. Jeong *et al.* improved the drilling ability of the HR by utilizing both magnetic torque and force under a precessional and gradient magnetic field [15]. Although the HR can unclog the clogged area, it takes a long time to drill through the clogged area. Drug-enhanced drilling motion has been investigated to improve drilling ability [16], [17]. Jeon *et al.* proposed a double HR, which contains the drug between double helical blades [16]. However, the drug may leak out during navigating motion because the small hole or nozzle in the robot is exposed to external fluid and lacks a sealing mechanism. Kim *et al.* developed a HR with active drug-release motion, in which the drug is sealed until active drug-release [17]. The robot utilizes two helical threads in the opposite direction, and the two propulsive forces in the opposite direction can open the drug chamber at the target area. However, one of the propulsive forces degrades the navigating ability of the HR because it generates a backward motion when it opens

Manuscript received June 17, 2017; revised August 15, 2017; accepted October 1, 2017. Date of publication October 9, 2017; date of current version December 13, 2017. Recommended by Technical Editor W. Li. This work was supported in part by the National Research Foundation of Korea funded by the Korean Government (MSIP) under Grant 2015R1A2A1A05001837. *(Corresponding Author: Gunhee Jang.)*

J. Nam, W. Lee, and J. Kim are with the Graduate School of Hanyang University, Seoul 04763, Korea (e-mail: njk0651@naver.com; justinleews@gmail.com; vmflvpseh@naver.com).

G. Jang is with the School of Mechanical Engineering, Hanyang University, Seoul 04763, Korea (e-mail: ghjang@hanyang.ac.kr).

This paper has supplementary downloadable material available at http://ieeexplore.ieee.org

Color versions of one or more of the figures in this paper are available online at http://ieeexplore.ieee.org.

Digital Object Identifier 10.1109/TMECH.2017.2761786

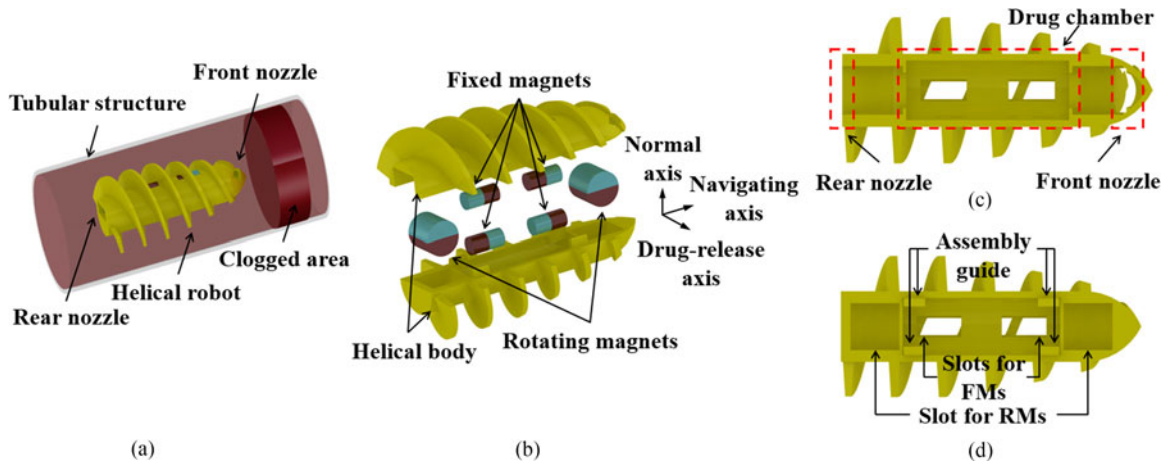

Fig. 1. (a) Proposed HR in the tubular structure with the clogged area. (b) Components of the HR. (c) Front and rear nozzles, and drug chamber in upper part of the helical body. (d) Slots for RMs and FMs, and assembly guide in lower parts of the helical body.

the chamber. Also, this robot cannot generate an independent drug-release motion. The drug-release mechanism always generated a propulsive navigating force, which may impede precise drug-delivery.

In this paper, we propose a novel HR with independent navigating, drug-release and drilling motions. The proposed HR is composed of two rotating cylindrical magnets (RMs), four fixed cylindrical magnets (FMs), and a helical body as shown in Fig. 1. The HR can perform independent propulsive (navigating and drilling motions) and drug-release motions utilizing two orthogonal magnetic torques generated by the application of two orthogonal external rotating magnetic fields (ERMFs). We designed the external magnetic field, RMs, and FMs, in such a way that the RMs can both tightly close the nozzle and discharge the drug during the navigating and drug-release motion, respectively. We then verified the various motions of the HR including the navigating, drug-release, and drilling motions. The drug-enhanced drilling motion was also demonstrated to show its effectiveness.

II. Principle of Manipulation

A. Structure of the HR

The proposed HR is composed of a helical body, two cylindrical RMs, and four cylindrical FMs as shown in Fig. 1(b). To assemble the RMs and FMs into the helical body, the helical body was divided into two parts as shown in Fig. 1(c) and (d). The divided parts were precisely assembled with four assembly guides to prevent drug leakage through the gap between the two parts. The helical body had a drug chamber to contain the drug. The front nozzle in the upper part of the helical body discharges the drug in the drug chamber, and the rear nozzle absorbs the external fluid into the drug chamber as shown in Fig. 1(c). We will explain in Section II-D how the front and rear nozzles discharge the drug and absorb the external fluid. The FMs were bonded to the helical body, while the slots of the RMs were slightly larger than the RM so that the inserted RMs can freely rotate in the slots along the drug-release axis to effectively squeeze and discharge the drug.

B. Magnetic Navigation System (MNS)

We constructed an MNS to manipulate the proposed HR as shown in Fig. 2(a) [7]. The MNS is composed of three coils, including one Helmholtz coil and two uniform saddle coils. Each coil generates an x-, y-, and z-directional uniform magnetic field near the center of the MNS. The magnetic field $(\mathbf{B_e})$ generated by the MNS can be expressed as follows [7]:

$$\mathbf{B_e} = \left[\frac{0.72 I_h}{r_h} \quad \frac{0.60 I_{uy}}{r_{uy}} \quad \frac{0.60 I_{uz}}{r_{uz}} \right]^T \tag{1}$$

where I_k and r_k are the current and radius of the kth coil, and the subscripts h, uy, and uz represent the Helmholtz coil, y-directional uniform saddle coil, and z-directional uniform saddle coil, respectively. Assuming that an alternating voltage (V_k) is applied to each coil, a current in (1) is determined by an impedance (Z_k) of a coil as follows [18]:

$$I_k = V_k / Z_k \tag{2}$$

$$Z_k = \sqrt{R_k^2 + (2\pi f L_k)^2} \tag{3}$$

where f, R_k, and L_k are the frequency of the alternating voltage, and the resistance and inductance of the k*th* coil, respectively. Using (1)–(3), we can determine the input voltage vector $(\mathbf{V}_i)$ to generate the required external magnetic field $(\mathbf{B_e})$ as follows:

$$\mathbf{V}_i = \begin{bmatrix} 0.72/Z_h r_h & 0 & 0 \\ 0 & 0.60/Z_{uy} r_{uy} & 0 \\ 0 & 0 & 0.60/Z_{uz} r_{uz} \end{bmatrix}^{-1} \mathbf{B_e}. \tag{4}$$

Table I shows the major design and operating values of the constructed MNS. Using (4) and Table I, we can calculate the magnetic flux densities according to the frequency as shown in Fig. 2(b). Considering time-varying magnetic field such as ERMF, we should calculate input voltage in real time and apply it to the MNS.

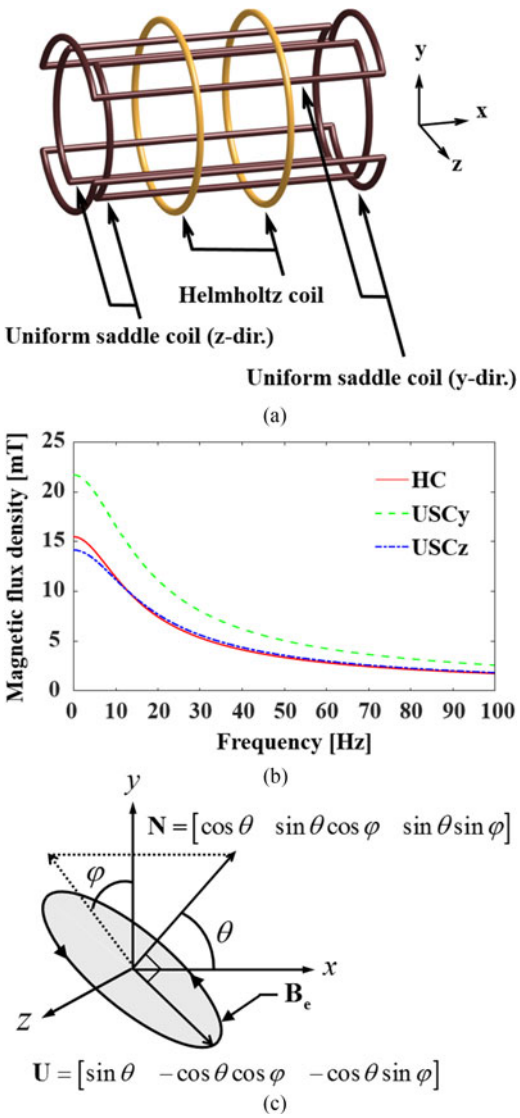

Fig. 2. (a) MNS composed of one Helmholtz coil and two uniform saddle coils to generate the ERMF. (b) Magnetic flux density generated by the MNS according to the frequency. (c) ERMF along unit vector **N**, and **U**, which is the unit vector normal to **N**.

TABLE I
MAJOR DESIGN AND OPERATING VALUES OF THE MNS

	HC	USCy	USCz
Turns of the coil (turns)	430	320	400
Radius of the coil (mm)	216.0	133.8	167.5
Resistance of the coil (Ω)	23.7	15.1	32.2
Inductance of the coil (mH)	344.5	201.3	394.3
Maximum input voltage (V)	218.5	178.1	251.2

C. Navigating and Drilling Motion

A magnet under an external magnetic field experiences magnetic torque as follows:

$$\mathbf{T_e} = \mathbf{m} \times \mathbf{B_e} \tag{5}$$

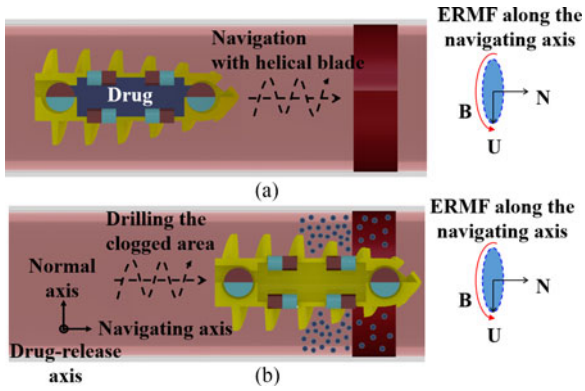

Fig. 3. (a) Navigating motion under the ERMF along the navigating axis. (b) Drilling motion under the ERMF along the navigating axis.

where **m** is the magnetic moment of a magnet and an external magnetic field, respectively. Once an ERMF is applied to a magnet, the magnetic torque in (5) generates a rotating motion of a magnet along the ERMF as shown in Fig. 2(c), and the ERMF can be expressed as follows:

$$\mathbf{B_e}(t) = B_0(\cos(2\pi ft)\,\mathbf{U} + \sin(2\pi ft)\,\mathbf{N} \times \mathbf{U}) \tag{6}$$

where B_0, f, **N**, and **U** are the magnitude and rotating frequency of the ERMF, the unit vector of the rotating axis, and the unit vector normal to **N**, respectively. The unit vectors (**N** and **U**) are expressed using θ and ϕ, which represent the angle between **N** and the x-axis, and the angle between the projection of **N** to the yz-plane and the y-axis. Fig. 3(a) and (b) shows the navigating and drilling motion under the ERMF along the navigating axis. The RMs rotate together with the helical body because the rotation of the RMs along the navigating axis is constrained by the helical body. Because the RMs and helical body rotate together, the HR can navigate or drill the clogged area with the helical blade.

D. Drug Seal and Release

We assume that the distance between the FMs and RMs is large enough to utilize the magnetic dipole model [19]. Then, the magnetic force ($\mathbf{F_{ab}}$) exerted on a dipole b by a dipole a can be expressed as follows [20]:

$$\mathbf{F_{ab}} = \frac{3\mu_0}{4\pi r^4}\left((\mathbf{r}\times\mathbf{m_a})\times\mathbf{m_b} + (\mathbf{r}\times\mathbf{m_b})\times\mathbf{m_a} - 2\mathbf{r}(\mathbf{m_a}\cdot\mathbf{m_b}) + 5\mathbf{r}((\mathbf{r}\times\mathbf{m_a})\cdot(\mathbf{r}\times\mathbf{m_b}))\right) \tag{7}$$

where μ_0, $\mathbf{r}$, r, $\mathbf{m_a}$, and $\mathbf{m_b}$ are the permeability of free space, the vector and the magnitude from dipole a to dipole b, and the magnetic moment of dipoles a and b, respectively. We can utilize this attractive magnetic force between the RMs and FMs to seal the nozzles at the front and rear parts of the HR. Fig. 4(a) shows that the attractive magnetic force between the RMs and FMs closes the nozzle. The ERMF can rotate the RMs in such a way that their magnetization direction is 90° with respect to the navigating axis to maximize this attractive magnetic force to seal the nozzles. The relative positions between the RMs and FMs during the navigation motion are as shown in Fig. 4(a).

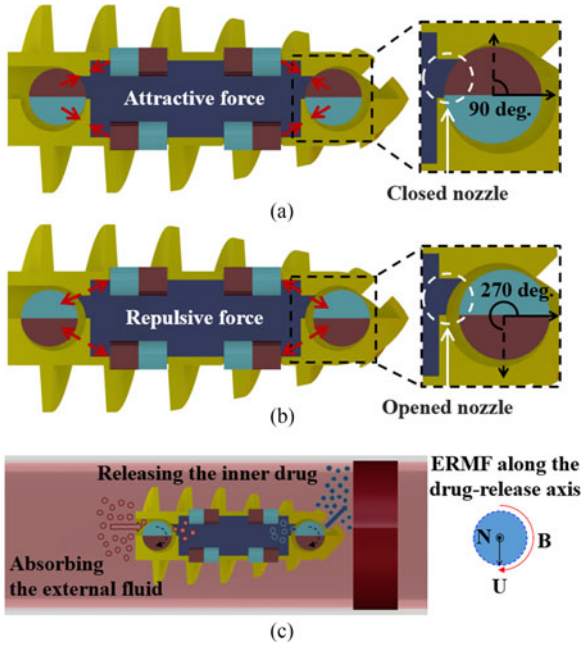

Fig. 4. (a) Attractive magnetic force to close the nozzles during the navigating motion. (b) Repulsive magnetic force to open the nozzles during the drug-release motion. (c) Drug-release motion under the ERMF along the drug-release axis.

The internal magnetic torque ($\mathbf{T_{ab}}$) exerted on dipole b by dipole a can be expressed as follows [20]:

$$\mathbf{T_{ab}} = \mathbf{m_b} \times \mathbf{B_a} \tag{8}$$

$$\mathbf{B_a} = \frac{\mu_0}{4\pi}\left(\frac{3\mathbf{r}(\mathbf{m_a}\cdot\mathbf{r})}{r^5} - \frac{\mathbf{m_a}}{r^3}\right) \tag{9}$$

where $\mathbf{B_a}$ is the magnetic flux density originating from magnet a. Once we apply the ERMF, if the external magnetic torque in (5) is greater than the internal magnetic torque between magnets in (8), the RMs can start to rotate. Fig. 4(b) shows that the repulsive magnetic force between the RMs and FMs opens the nozzle. The ERMF can rotate the RMs in such a way that their magnetization direction is 270° with respect to the navigating axis. This maximizes the repulsive magnetic force to open the nozzles. If we apply the ERMF along the drug-release axis, as shown in Fig. 4(c), the RMs eccentrically and repeatedly rotate. This motion discharges the drug in the slot of the front RM through the front nozzle. It also sucks the external fluid around the rear RM into the drug chamber through the rear nozzle. Although the drug can be released only through the front nozzle, the rear nozzle contributes to circulation by allowing passage of the fluid. The drug can be smoothly released using the front and rear nozzles.

III. Design of the HR

Table II shows the magnetic properties of the RMs and FMs of the HR. Once we determined the magnetic moment of the RMs and FMs, the magnetic flux density originating from the FMs was determined from the distance between the RMs and the FMs (D). The ERMF was also determined from the applied

TABLE II
Properties of the Magnets

Property	Rotating Magnet	Fixed Magnet
Type	Cylinder	Cylinder
Magnetization direction	Radial direction	Axial direction
Residual magnetic flux density	1.45 T	1.45 T
Magnetic moment	$7.25\,\mathrm{mA}-\mathrm{m}^2$	$1.81\,\mathrm{mA}-\mathrm{m}^2$
Diameter	2 mm	1 mm
Length	2 mm	2 mm

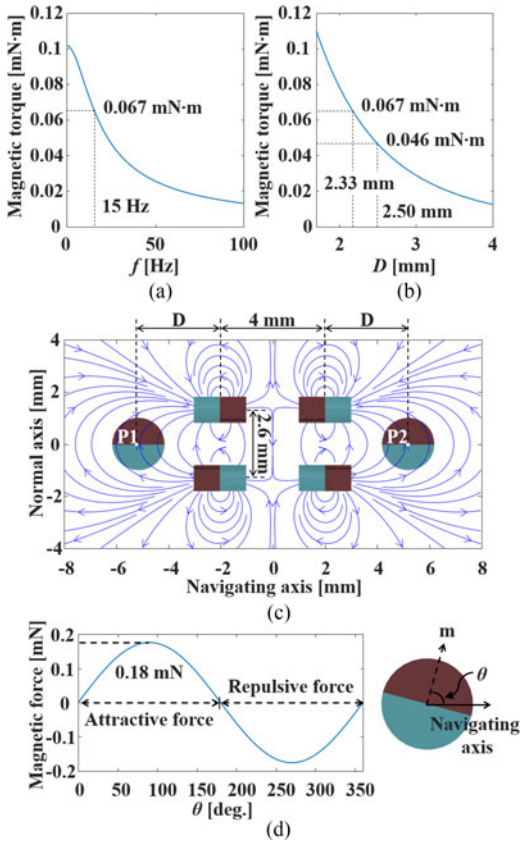

Fig. 5. (a) Magnetic torque applied to each RM by the ERMF along the drug-release axis according to the frequency of the ERMF. (b) Magnetic torque applied to each RM by the FMs according to the distance between the RMs and FMs. (c) Magnetic field distribution by the FMs. (d) Magnetic force applied from the FMs to each RM according to θ between the magnetic moment of the RMs and navigating axis.

current of the MNS. To open and close the nozzles by rotating the RMs, we determined D in such a way that the magnetic torque from the ERMF was greater than that from the FMs. Utilizing (1)–(3), (5), (8), (9), and Tables I and II, we can calculate $\mathbf{T_e}$ and $\mathbf{T_{ab}}$, as shown in Fig. 5(a) and (b) while the both magnetic torques are the peak values in the case that the magnetization direction of the RMs is 90° with respect to the applied magnetic field. Because the amplitude of the ERMF was determined by the minimum magnetic field of the coils of the MNS, we used the magnetic field generated by the z-directional uniform saddle coil to calculate $\mathbf{T_e}$. The value of $\mathbf{T_e}$ decreases as the frequency increases, as shown in Fig. 2(b). Therefore, we first set the

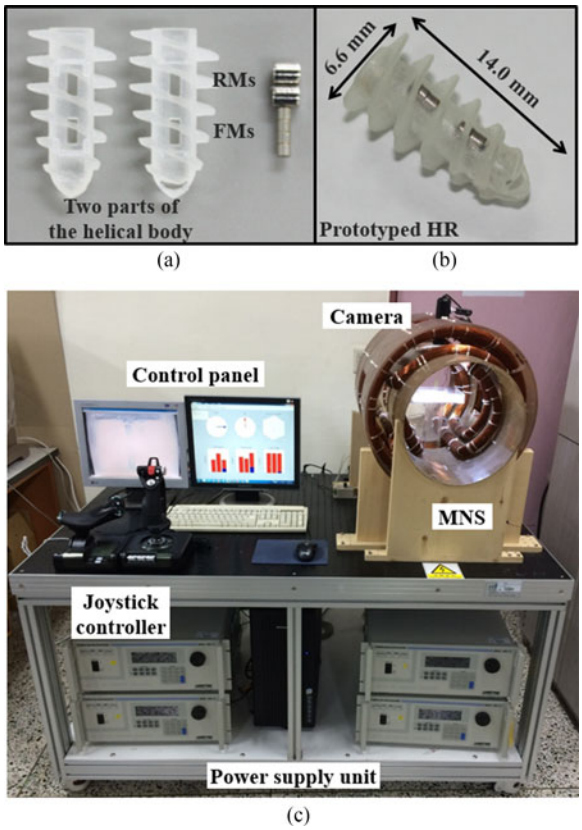

Fig. 6. (a) Components of the prototyped HR. (b) Assembled HR with a diameter of 6.6 mm and length of 14.0 mm. (c) Experimental setup to manipulate the proposed HR.

frequency range for drug-release as 0 to 15 Hz. Then, D should be larger than 2.33 mm for this frequency range. However, we selected D to be 2.50 mm, which is slightly larger than 2.33 mm, to account for friction, manufacturing and assembly errors.

Fig. 5(c) shows the distribution of the magnetic field by the four FMs using the superposition of (9), and the magnetic field was generated along the normal axis at the centers of the RMs ($P1$ and $P2$). Because the magnetic torque exerted on the RMs by the FMs in (6) has the same direction as the external magnetic field, the RMs aligned with the magnetic field ($\theta = 90°$). Fig. 5(d) shows the calculated magnetic force from the FMs to each RM as a function of the rotating angle. The attractive magnetic force is generated in the range from 0° to 180° to close the nozzles, while the repulsive magnetic force is generated in the range from 180° to 360° to open the nozzles. The aligned RMs can seal the nozzle with a maximum magnetic force of 0.18 mN.

IV. Results and Discussion

We prototyped the helical body of the proposed HR with a multijet-modeling-based three-dimensional (3-D) printing technology using an ultraviolet-curable acrylic plastic material as shown in Fig. 6(a). The maximum printing error per unit thickness was 2 μm/mm. Fig. 6(b) shows the assembled HR, which is 6.6 mm in diameter and 14.0-mm-long, and Fig. 6(c)

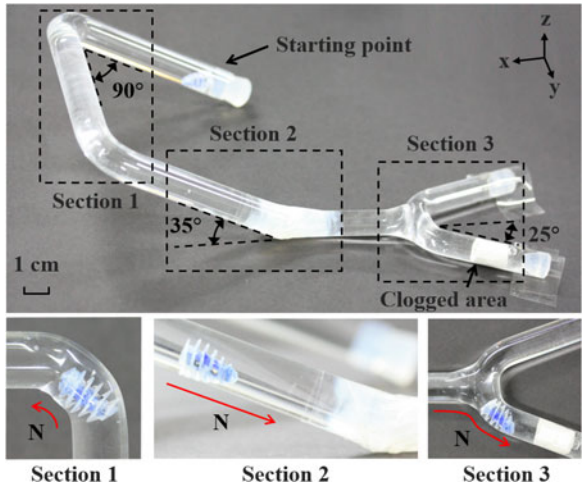

Fig. 7. Navigating motion of the HR in the complex tubular environment by controlling the vector **N** of the ERMF.

shows the constructed experimental setup to verify the proposed HR. The proposed HR was manipulated by a joystick controller inside the MNS and tracked by a real-time camera. To verify the proposed design, we rotated the RMs under the ERMF of 14 mT along the drug-release axis. With the design variable D of 2.5 mm, the RMs could be rotated up to a frequency of 15.4 Hz, which matches well with the calculated frequency of 15.0 Hz.

The proposed HR has navigating, drug-release, and drilling capability. At first, we verified navigating capability of the proposed HR in a watery 3-D bifurcated tubular environment whose inner diameter of 7 mm is anatomically similar to several vascular environments such as large coronary arteries, abdominal aorta, femoral arteries, and carotid arteries (diameter of 7 to 15 mm) [21], [22]. During the experiment, we utilized the ERMF whose amplitude and frequency are 9.1 mT and 15 Hz, and steered the HR by controlling the vector **N** of the ERMF in (6) along the moving direction. The desired voltage vector was also calculated in real-time utilizing the ERMF in (4), and the calculated voltage vector was applied to each coil of the MNS. Fig. 7 shows the navigating motion of the HR in the complex tubular environment which includes inclined, horizontal, and bifurcated passages (see supplemental video). In Section I, the HR moved upward along the inclined tube with the slope angle of 35°, turned left at the corner and moved forward along the horizontal tube. Then, the HR turned left again at the second corner, moved downward along the inclined tube with the slope angle of 35° in Section II and moved forward along the horizontal tube. Finally, the HR reached the bifurcated area in Section III, and it went to the right side to reach the clogged area. During the navigation, we could observed that the drug was tightly sealed by the attractive magnetic force between the magnets.

We also verified the drug-release capability of the HR by measuring the drug-release time according to the frequency of the ERMF. To clearly observe the released drug, we separate the front and rear nozzles utilizing two tube, which has different diameters as shown in Fig. 8(a). In this figure, the right sides of the proposed HR are tightly connected to the watery glass tube, which had inner diameters of 9 and 6 mm, respectively.

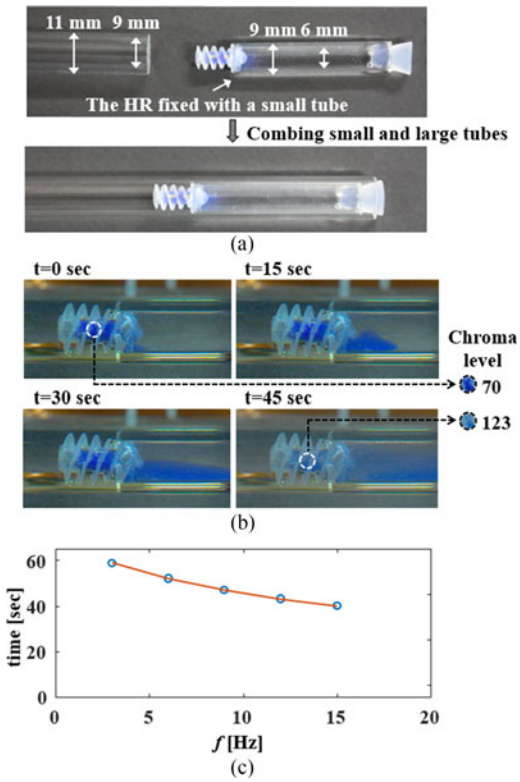

Fig. 8. (a) Experimental setup to verify the drug-release capability. (b) One of the drug-release motion ($B_0 = 11.6\,\mathrm{mT}$, $f = 9\,\mathrm{Hz}$). (c) Required time to release the drug according to frequency.

Then, the tube was inserted into the larger tube, which had inner diameters of 11 and 9 mm. In this way, we observed the discharged colored drug in the right watery glass tube due to the eccentric rotational motion of the RMs. To measure the required time for the drug-release, we captured the drug-release motion using a video camera. As the drug-release motion progresses, the chroma level increases because the drug is discharged through the front nozzle and the water flows into the drug chamber. We measured the chroma level in the middle of the drug chamber until the chroma level increased over 75% in comparison with the initial level. Fig. 8(b) shows one of the drug-release motions, and we observed an increase in chroma level over time because the drug was released through the front nozzle. Fig. 8(c) shows the measured required time as a function of the frequency of the ERMF, and it shows that the high frequency of the ERMF generates a rapid drug-release motion. However, the drug could not be released at frequencies over 15 Hz because the ERMF could not generate a magnetic torque enough to overcome the magnetic torque between the FMs and RMs.

We also conducted an experiment to measure the propulsive force, which affects the navigating and drilling capabilities of the HR. Fig. 9(a) shows the constructed experimental setup. The glass tube containing the HR was fixed in a water container, and a jig connected to the load cell (*Model 31 of Honeywell, USA*) was placed in front of the glass tube. The experimental setup was then placed inside of the MNS. Once the ERMF generated from the MNS was applied to the HR, the propulsive force of the HR was measured by the load cell. Fig. 9(b) shows two ERMFs

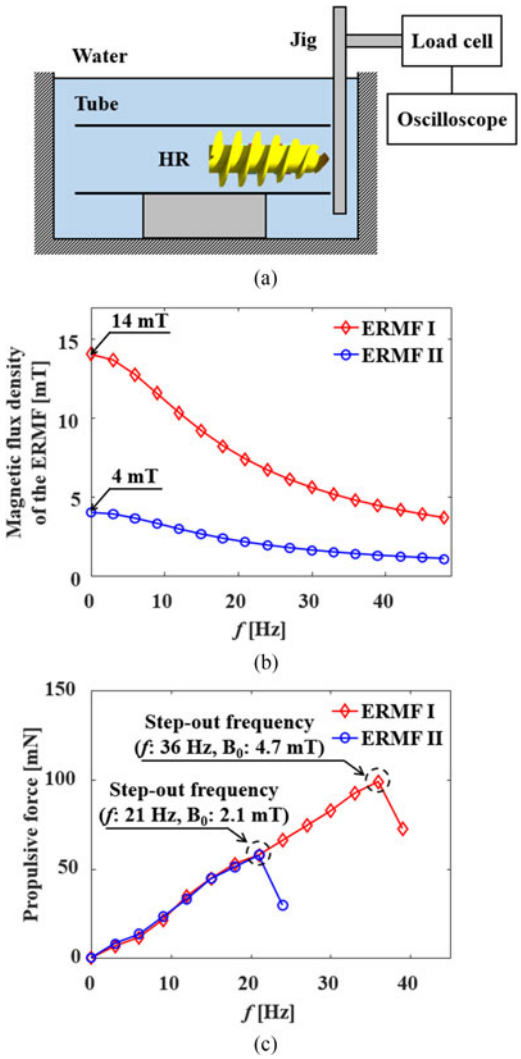

Fig. 9. (a) Experimental setup to measure the propulsive force of the HR. (b) Magnetic flux densities of two ERMFs according to their rotational frequency while they have different initial values of 14 and 4 mT, respectively. (c) Propulsive force of the HR according to the amplitude and frequency of the ERMF.

with initial magnetic flux densities of 14 and 4 mT according to rotational frequency and it shows that they decrease with the increase of rotating frequency due to the inductance effect in (3). Fig. 9(c) shows the measured propulsive force of the HR according to rotational frequency. It shows that the propulsive force is proportional to the rotational frequency until it reached the step-out frequency. However, over the step-out frequency, the propulsive force decreases because the HR could not be synchronized with the ERMF [23], [24]. We also observed that the ERMF with initial magnetic flux densities of 14 mT could generate the maximum unclogging force of 100 mN with the step-out frequency of 36 Hz. This unclogging force can unclog the soft chronic total occlusion, which is one of our target lesion [25], [26]. Utilizing these experimental results, the unclogging motion should be cautiously and precisely generated in actual situation because the mechanical drilling may damage a lesion of the clogged area and cause embolism.

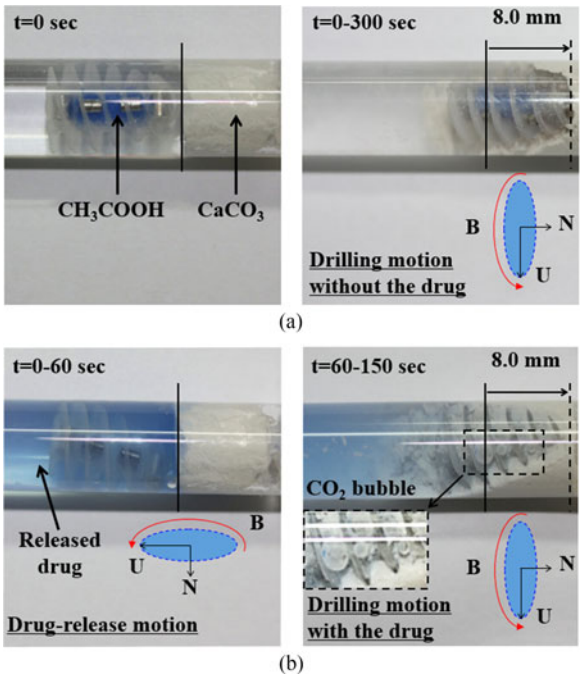

Fig. 10. (a) Drilling motion of the HR without drug-release. (b) Drilling motion of the HR after drug-release motion.

Finally, we conducted an experiment to show the effectiveness of the drug-enhanced drilling. In the experiment, the drilling capability of the HR was compared according to the presence of the drug. To simulate the clogged vascular environment, we blocked the end of the tube with a cylindrical solid calcium carbonate ($CaCO_3$) with a diameter and length of 7 and 8 mm. As the drug, we loaded liquid acetic acid (CH_3COOH, 40% transparent aqueous solution) with blue dye into the drug chamber of the prototyped HR. We can observe CO_2 gas in the case that $CaCO_3$ successfully reacts with the CH_3COOH. Fig. 10(a) shows the drilling motion without drug-release, while Fig. 10(b) shows the drilling motion after the drug-release (see supplemental video). During the drug-release motion, we observed slight vibration of the HR due to the magnetic torque between the RMs and FMs because the rotational motion of the RMs generates magnetic torque on the FMs in (8). However, it did not disturb the drug release motion in this experiment where the length of the HR was longer than the diameter of the tube because the HR was constrained along the tube and closely contacted with the wall of the tube. We utilized the ERMF with the amplitude and frequency of 13.7 mT and 3 Hz for drug-release motion, and it could stably release the drug as shown in Fig. 10(b). In the experiment, the HR with the drug could unclog the $CaCO_3$ in 90 s, while the HR without the drug took 300 s to unclog the $CaCO_3$. This experiment shows the possibility that the proposed HR could deliver drug without leakage and effectively unclog tubular structures in the human body.

V. Conclusion

We developed a novel HR that can perform targeted drug-delivery without drug leakage. We utilized two orthogonal ERMFs along the moving direction to generate navigating, drilling, and drug-release motions. In the navigating and drilling motions, the magnetic torque and the attractive magnetic force between RMs and FMs tightly seals the nozzles in the drug chamber. In the drug-release motion, we applied an ERMF orthogonal to the moving direction to eccentrically rotate the RMs due to the interaction of the FMs in such a way that the drug in the slot of the front RMs is squeezed and discharged through the front nozzle. At the same time, the external fluid near the rear RM is sucked through the rear nozzle. We designed and prototyped the HR to verify its targeted drug-delivery capability. We performed several experiments and verified the navigating, drug-release, and drilling capabilities. This research will contribute to treating the diseases required to deliver drug through the tubular structure of human body such as targeted anticancer drug delivery to liver cancer or antihemorrhagic agent delivery to brain hemorrhage or lung to cause hemoptysis. There are still several technical challenges before clinical trial or commercialization of magnetic robots such as developing a multifunctional magnetic robot, an MNS to generate strong magnetic field, and real-time visualization or tracking of a magnetic robot inside human body.

References

[1] S. Saito *et al.*, "Angioplasty for chronic total occlusion by using tapered-tip guidewires," *Catheter. Cardiovasc. Interv.*, vol. 59, no. 3, pp. 305–311, Jul. 2003.
[2] F. Tendick, S. S. Sastry, R. S. Fearing, and M. Cohn, "Applications of micromechatronics in minimally invasive surgery," *IEEE/ASME Trans. Mechatronics*, vol. 3, no. 1, pp. 34–42, Mar. 1998.
[3] S. Hasanzadeh and F. Janabi-Sharifi, "Model-based force estimation for intracardiac catheters," *IEEE/ASME Trans. Mechatronics*, vol. 21, no. 1, pp. 154–162, Feb. 2016.
[4] R. Cappato *et al.*, "Up-dated worldwide survey on the methods, efficacy and safety of catheter ablation for human atrial fibrillation," *Circ. Arrhythm. Electrophysiol.*, vol. 3, pp. 32–38, Jan. 2009.
[5] L. Venneri *et al.*, "Cancer risk from professional exposure in staff working in cardiac catheterization laboratory: Insights from the National Research Council's Biological Effects of Ionizing Radiation VII Report," *Amer. Heart J.*, vol. 157, no. 1, pp. 118–124, Jan. 2009.
[6] H. Choi, J. Choi, S. Jeong, C. Yu, J. Park, and S. Park, "Two-dimensional locomotion of a microrobot with a novel stationary electromagnetic actuation system," *Smart Mater. Struct.*, vol. 18, no. 11, 2009, Art. no. 115017.
[7] S. Jeon, G. Jang, H. Choi, and S. Park, "Magnetic navigation system with gradient and uniform saddle coils for the wireless manipulation of micro-robots in human blood vessels," *IEEE Trans. Magn.*, vol. 46, no. 6, pp. 1943–1946, Jun. 2010.
[8] W. Ma, J. Li, F. Niu, H. Ji, and D. Sun, "Robust control to manipulate a microparticle with electromagnetic coil system," *IEEE Trans. Ind. Electron.*, vol. 64, no. 11, pp. 8566–8577, Nov. 2017.
[9] J. Nam, W. Lee, B. Jang, and G. Jang, "Magnetic navigation system utilizing resonant effect to enhance magnetic field applied to magnetic robots," *IEEE Trans. Ind. Electron.*, vol. 64, no. 6, pp. 4701–4709, Jun. 2017.
[10] S. Yim, K. Goyal, and M. Sitti, "Magnetically actuated soft capsule with the multimodal drug release function," *IEEE/ASME Trans. Mechatronics*, vol. 18, no. 4, pp. 1413–1418, Aug. 2013.
[11] J. Nam, S. Jeon, S. Kim, and G. Jang, "Crawling microrobot actuated by a magnetic navigation system in tubular environments," *Sens. Actuators Phys.*, vol. 209, pp. 100–106, Mar. 2014.
[12] K. Ishiyama, M. Sendoh, and K. I. Arai, "Magnetic micromachines for medical applications," *J. Magn. Magn. Mater.*, vol. 242–245, pp. 41–46, Apr. 2002.
[13] S. H. Kim, S. Hashi, and K. Ishiyama, "Hybrid magnetic mechanism for active locomotion based on inchworm motion," *Smart Mater. Struct.*, vol. 22, no. 2, 2013, Art. no. 027001.
[14] T. Fukushi, S. Hoon Kim, S. Hashi, and K. Ishiyama, "Preliminary validation of Sm-Fe-N magnetic silicone rubber for a flexible magnetic actuator," *Smart Mater. Struct.*, vol. 23, no. 6, 2014, Art. no. 067001.

[15] S. Jeong, H. Choi, K. Cha, J. Li, J. Park, and S. Park, "Enhanced locomotive and drilling microrobot using precessional and gradient magnetic field," *Sens. Actuators Phys.*, vol. 171, no. 2, pp. 429–435, Nov. 2011.
[16] S. M. Jeon, G. H. Jang, and W. S. Lee, "Drug-enhanced unclogging motions of a double helical magnetic micromachine for occlusive vascular diseases," *IEEE Trans. Magn.*, vol. 50, no. 11, pp. 1–4, Nov. 2014.
[17] S. H. Kim and K. Ishiyama, "Magnetic robot and manipulation for active-locomotion with targeted drug release," *IEEE/ASME Trans. Mechatronics*, vol. 19, no. 5, pp. 1651–1659, Oct. 2014.
[18] D. Halliday, R. Resnick, and J. Walker, *Fundamentals of Physics Extended*. Hoboken, NJ, USA: Wiley, 2010.
[19] A. J. Petruska and J. J. Abbott, "Optimal permanent-magnet geometries for dipole field approximation," *IEEE Trans. Magn.*, vol. 49, no. 2, pp. 811–819, Feb. 2013.
[20] D. D. Villani, "An analytic solution for the force between two magnetic dipoles," *Magn. Elect. Sep.*, vol. 9, pp. 39–52, 1998.
[21] H. Kahraman *et al.*, "The diameters of the aorta and its major branches in patients with isolated coronary artery ectasia," *Tex. Heart Inst. J.*, vol. 33, no. 4, pp. 463–468, 2006.
[22] T. Sandgren, B. Sonesson, Å. R. Ahlgren, and T. Länne, "The diameter of the common femoral artery in healthy human: Influence of sex, age, and body size," *J. Vasc. Surg.*, vol. 29, no. 3, pp. 503–510, Mar. 1999.
[23] K. Ishiyama, M. Sendoh, A. Yamazaki, and K. I. Arai, "Swimming micromachine driven by magnetic torque," *Sens. Actuators Phys.*, vol. 91, no. 1/2, pp. 141–144, Jun. 2001.
[24] F. Qiu and B. J. Nelson, "Magnetic helical micro- and nanorobots: Toward their biomedical applications," *Engineering*, vol. 1, no. 1, pp. 21–26, Mar. 2015.
[25] T. Roy, G. Liu, N. Shaikh, A. D. Dueck, and G. A. Wright, "Puncturing plaques: Relating MRI characteristics of peripheral artery lesions to guidewire puncture forces," *J. Endovasc. Therapy*, vol. 24, no. 1, pp. 35–46, 2017.
[26] H. Saito and T. Togawa, "Detection of needle puncture to blood vessel using puncture force measurement," *Med. Biol. Eng. Comput.*, vol. 43, no. 2, pp. 240–244, Apr. 2005.

Jaekwang Nam received the B.S. degree in mechanical engineering from Hanyang University, Seoul, South Korea, in 2011. He is currently working toward the Ph.D. degree in mechanical convergence engineering with the Department of Mechanical Convergence Engineering, Hanyang University.

His research interests include various structures of the magnetic robot performing multifunction in human blood vessels and its magnetic navigation system.

Wonseo Lee (S'16) received the B.S. degree in mechanical engineering from Hanyang University, Seoul, South Korea, in 2014. He is currently working toward the Ph.D. degree in mechanical convergence engineering with Hanyang University.

His current research interests include design, analysis, and control of magnetic robots and magnetic catheters with electromagnetic systems for biomedical applications.

Jongyul Kim received the B.S. degree in mechanical engineering from Hanyang University, Seoul, South Korea, in 2016. He is currently working toward the Ph.D. degree in mechanical convergence engineering with the Department of Mechanical Convergence Engineering, Hanyang University.

His research interests include control mechanism of magentic robot in the magnetic navigation system for multipurpose therapeutic treatment.

Gunhee Jang (M'00) received the B.S. degree in mechanical engineering from Hanyang University, Seoul, South Korea, in 1984; the M.S. degree in mechanical engineering from the Korea Advanced Institute of Science and Technology, Seoul, in 1986; and the Ph.D. degree in mechanical engineering from the University of California, Berkeley, CA, USA, in 1993.

He is currently a Professor with the Department of Mechanical Engineering and the Director of the Precision Rotating Electromechanical Machine Laboratory, Hanyang University. His current research interests include the magnetic robot actuated by magnetic navigation system and electromechanical systems such as motors and actuators. He has authored or co-authored more than 280 articles published in journals and conferences in his field, and more than 29 patents including several international patents.